

Coherent Transport of Atomic Quantum States in a Scalable Shift Register

A. Lengwenus, J. Kruse, M. Schlosser, S. Tichelmann, and G. Birkl*

Institut für Angewandte Physik, Technische Universität Darmstadt, 64289 Darmstadt, Germany
(Received 4 March 2009; revised manuscript received 31 August 2010; published 22 October 2010)

We demonstrate the coherent transport of 2D arrays of small ensembles of neutral atoms in a shift register architecture based on 2D arrays of microlenses. We show the scalability of the transport process by presenting the repeated hand over of atoms from site to site. We prove the conservation of coherence during transport, reloading, and a full shift register cycle. This shows that the fundamental shift sequence can be cascaded and thus scaled to complex and versatile 2D architectures for atom-based quantum information processing, quantum simulation, and the investigation of quantum degenerate gases.

DOI: 10.1103/PhysRevLett.105.170502

PACS numbers: 03.67.Lx, 37.10.Jk, 42.50.Ex

In many of the recent advances in the investigation of quantum degenerate gases and neutral atom quantum information processing, versatile architectures for the coherent storage and transport of atomic quantum systems based on optical dipole potentials play a crucial role [1–11]. Specifically, the application of standing-wave configurations (optical lattices) [1–6] and single or multiple focused laser beams [7–11] has led to significant progress in the manipulation of atomic qubit states for quantum information processing. In our work, we focus on the implementation of geometries based on microfabricated optical elements [8,12–14]. This approach allows us to develop flexible and integrable configurations for quantum-state storage and manipulation, simultaneously targeting the important issues of single-site addressing and scalability, essential to most architectures for quantum information processing [15] and quantum simulation. The scalable shift register presented here is an all optical device which offers precise control of the transport of trapped neutral atoms in a 2D architecture. The atoms are localized in miniaturized arrays of dipole potentials created by 2D microfabricated lens structures [8,12]. The shift operation is based on consecutive loading, moving, and reloading of two independently controllable arrays of traps. Figure 1 shows a 2D register of about 25 atom samples [each able to carry one quantum bit (qubit) [14]] detected by collecting the fluorescence light emitted by the atoms when illuminated with a resonant laser pulse after 0, 1, 2, and 3 consecutive shift sequences. The shift register allows for atom transport over macroscopic distances and at the same time for controlled atom-atom approach with submicrometer precision which is necessary for the implementation of two-qubit quantum gates [16–24]. Moreover, it can serve as a two-dimensional quantum memory to archive and retrieve quantum information, or sequentially shuffle quantum information through complex architectures. Conservation of coherence of the quantum states and adiabaticity during transport are essential requirements that will be addressed in this Letter. An extension of the results for 1D shift operations presented here to 2D is straightforward. The

experiments presented here are performed with ^{85}Rb atoms inside a glass cell based vacuum system (Fig. 2). Each experimental sequence is initiated by preparing an ensemble of about 10^6 atoms in a standard retroreflected magneto-optical trap (MOT). The atoms are further cooled by optical molasses to approximately $10\ \mu\text{K}$ before being partially transferred into a superimposed 2D register of dipole traps. The traps are created by illuminating a subset of a two-dimensional array (A1) of 50×50 microfabricated refractive lenses with light far red detuned from the $D1$ and $D2$ transitions of Rb. The microlenses have a diameter of $100\ \mu\text{m}$, a pitch of $125\ \mu\text{m}$, and a focal length of $1\ \text{mm}$. The focal plane of the array is relayed into the glass cell using a telescope which consists of an achromatic lens ($L1$, $f = 80\ \text{mm}$) and a diffraction limited lens system (LS , $f = 35.5\ \text{mm}$, numerical aperture $NA = 0.29$). The demagnification results in traps with a separation of $a = 55\ \mu\text{m}$ and a measured waist of $3.8\ \mu\text{m}$ ($1/e^2$ radius). Illuminating the microlens array with a laser beam at $805\ \text{nm}$ wavelength, a power of $275\ \text{mW}$, and a $1/e^2$ radius of $450\ \mu\text{m}$ results in a two-dimensional array of traps with a power of $5.7\ \text{mW}$ and a depth of $k_B \times 430\ \mu\text{K}$ for the central trap. Here, the vibrational frequencies are $\Omega_r = 2\pi \times 17\ \text{kHz}$ for the radial and $\Omega_a = 2\pi \times 820\ \text{Hz}$ for the axial direction. About 200 atoms with a temperature of $15 \pm 1.5\ \mu\text{K}$ (measured by a time-of-flight technique) are trapped in the central trap. Because of the Gaussian profile of the laser beam illuminating the microlens array,

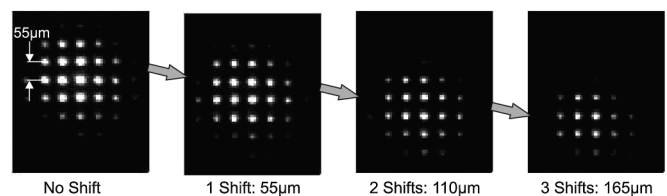


FIG. 1. Fluorescence images of 2D arrays of trapped atoms in a shift register based on 2D arrays of microlenses. Images are taken after 0, 1, 2, and 3 consecutive shift sequences of $55\ \mu\text{m}$ transport distance each.

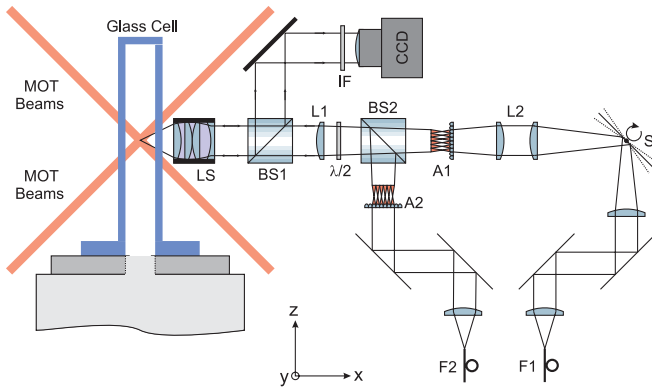


FIG. 2 (color online). Experimental setup. Microlens array A1 is illuminated with light delivered by optical fiber F1. The incident angle on A1 is controlled by scanning mirror S in combination with the transfer lenses L2. A second fixed array A2 is illuminated with light delivered by fiber F2. The focal planes of both arrays are superimposed by beam splitter BS2 and transferred by lens L1 and lens system (LS) into the MOT region. Detection of fluorescence light is performed through LS and beam splitter BS1 by a CCD camera with interference filter (IF) to block stray light.

the outlying traps are shallower. The number of traps loaded (here about 5×5) depends on this beam size and also on the size of the MOT. The lifetime of the atoms in the traps is on the order of 0.5 s, which is mainly limited by collisions with background gas atoms. Atom detection is achieved by resonance fluorescence imaging of the atom distribution using the MOT beams for illumination and collecting the fluorescence light with a CCD camera through lens system LS and beam splitter BS1.

To move the traps, we vary the incident angle on microlens array A1 by a feedback-controlled scanning mirror S which deflects the incoming beam. The pivot point of the beam on the scanning mirror is imaged onto the microlens array by telescope L2 with unity magnification. This causes the foci of the array to shift laterally within the focal plane as a function of the angle of the scanning mirror. It is straightforward to shift the array by a distance of the full trap separation of $55 \mu\text{m}$. Moving significantly more than this distance results in strong deformations of the trapping potentials by lens aberrations due to the skewed illumination of the microlenses. The angular reproducibility of the scanner is better than $22 \mu\text{rad}$, which implies that the trap position can be controlled to better than 10 nm.

A complete shift register sequence consists of consecutive loading, moving, and reloading of two independently controllable arrays of dipole traps. The fixed focal structure of microlens array A2 (identical to lens array A1) is combined with the movable focal structure of array A1 by beam splitter BS2. For shift and reloading durations of 5 ms, the timing sequence for the potential depths of arrays A1 and A2 and for the position of array A1 are shown in Fig. 3(a). The fluorescence images in Fig. 3(b) show the central column of the array of Fig. 1 as a function of time during

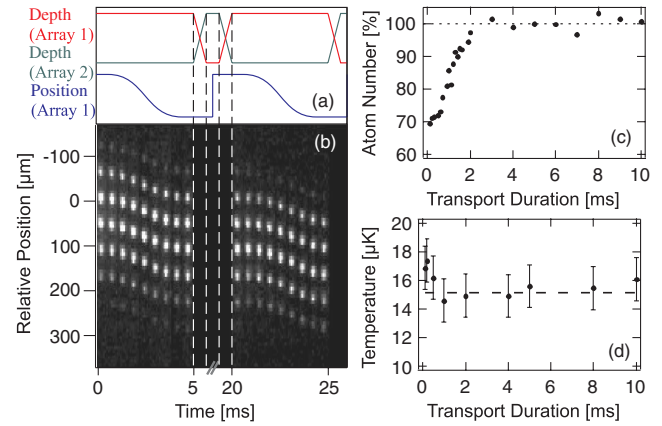


FIG. 3 (color online). (a) Timing sequence for depth and position of the two trap arrays constituting a shift register. (b) Fluorescence images of atoms in the central column of the register of Fig. 1 during two consecutive shift cycles. No images are shown for the phases of loading and reloading between the arrays and the phase of returning array A1 to its start position (5 ms each). (c) Atom number and (d) temperature in the central trap at the end of a single transport sequence of $55 \mu\text{m}$ distance as a function of the transport duration. The dashed line in (d) shows the temperature for a fixed trap. Each data point is averaged 15 times.

two consecutive shift cycles. The shift operation is comparable to a bucket chain: while A2 is switched off initially, we load atoms from the MOT into A1 at $-a/2$ and shift it by one full trap separation from $-a/2$ to $+a/2$ in a few ms. We transfer the atoms to A2 (illuminated under normal angle but laterally displaced by $+a/2$) by raising the intensity in A2 while ramping it down in A1. Then the scanning mirror is returned to its initial position which superimposes the next row of traps of A1 with the traps of A2. To complete a shift cycle, the atoms are reloaded from A2 to A1, and the next fully identical shift cycle can begin. The number of achievable shift sequences is only limited by the size of the illuminated trap array. The 5×5 trap array in this realization, for example, allows for 5 sequences and gives a final transfer distance of $275 \mu\text{m}$. For sufficient laser power, fully exploiting the here available set of 50×50 microlenses allows for atom transport over many trap separations.

Minimizing atom loss and heating are essential for the shift register and, e.g., also for specific realizations of quantum gates where atoms have to be brought close together and separated again [16–24]. For this reason, we investigated in detail heating and atom loss during individual transport operations. Figure 3 shows the atom number [3(c)] and temperature [3(d)] at the end of single transport sequences with varying duration. The transport distance is one full trap separation. Typical initial temperatures are $15 \pm 1.5 \mu\text{K}$. For transport durations above 1 ms we measure no increase in temperature, and for transport durations above 2 ms no atom loss. Heating and atom loss for faster transport arise from technical limitations of the scanning

mirror: for short scan times, the mirror has to be strongly accelerated and decelerated, causing the mirror to overshoot its final position because of its inertia. This results in oscillations around the final position which cause resonant excitation of the vibrational levels and as a consequence heating and atom loss. Optimization allowed us to minimize this effect by smoothing the ramps for acceleration and deceleration as shown in the trace for the position of array A1 in Fig. 3(a) and thus to reduce the required scan duration to 2 ms.

We also investigated atom loss and heating for a shift register consisting of several shift cycles. After a sequence of four cycles (Fig. 1), heating was measured to be below $2 \mu\text{K}$, which is comparable to our measurement uncertainty. On the other hand, atom loss on the order of 20% was encountered for each loading from A1 to A2, whereas no loss was observed for reloading from A2 to A1. In a separate series of measurements we found that this was caused by the fact that loading and reloading have not been fully symmetrical operations since A1 was displaced to $+a/2$ by tilted illumination whereas A2 was laterally moved to $+a/2$ but illuminated normal. This leads to slightly tighter traps in A2 as compared to A1. Minimizing this mismatch could be achieved through symmetrizing the loading and reloading processes by having both arrays displaced by $|a/2|$ with opposite sign through tilted illumination during the loading and reloading phases. This allows us to reload atoms in both directions without detectable loss. For quantum information processing in this architecture, the coherence of superpositions of quantum states also has to be preserved during transport, reloading, and the full shift cycle. In our approach, qubit states are represented by hyperfine substates of the $5S_{1/2}$ ground state of ^{85}Rb . To be insensitive to fluctuations of magnetic fields to first order, we prepare the atoms in the clock state ($F = 2$, $m_F = 0$), which we coherently couple to the second clock state ($F = 3$, $m_F = 0$) with a phase-locked diode laser system. The typical duration of an applied π pulse is $210 \mu\text{s}$. State-selective detection is performed by removal of the atoms in $F = 3$ and subsequent detection of the remaining atoms in $F = 2$.

We analyze the influence of atom transport on dephasing and decoherence by applying Ramsey and spin-echo methods. The trapping laser light is tuned to a wavelength of 815 nm with a power of 150 mW distributed over a beam with a $1/e^2$ radius of $520 \mu\text{m}$. For the central trap, this gives a power of 2.3 mW and a trap depth of $k_B \times 110 \mu\text{K}$. As the atom ensemble in each trap is thermal and thus distributed over a range of vibrational levels, each atom incurs a slightly different ac-Stark shift. This leads to inhomogeneous dephasing of the Ramsey signal already for atoms at rest [Fig. 4 (left)] with a time constant of about 5 ms. To compensate for this, we implemented a spin-echo technique which reverses inhomogeneous dephasing. This allows us to directly measure the combined time constant T'_2 of homogeneous dephasing and decoherence and thus to

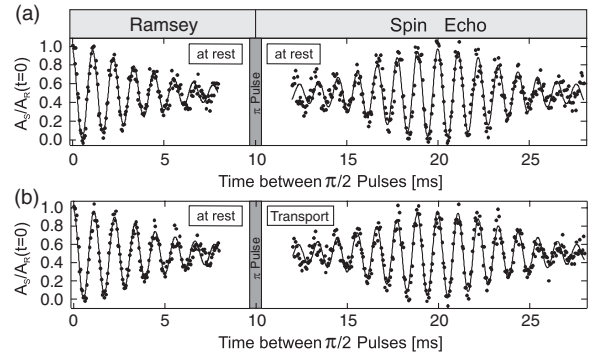


FIG. 4. Spin-echo measurements for atoms at rest [(a), right] and atoms transported over a distance of $55 \mu\text{m}$ [(b), right] in the central trap of a two-dimensional trap array. In both cases, the spin-echo signal (A_E) is normalized to the initial amplitude [$A_R(t = 0)$] of a Ramsey signal for atoms at rest (left). There is almost negligible additional loss of signal contrast through atom transport. Each data point is averaged 5 times.

compare the behavior of atoms at rest and atoms transported. For atoms at rest [Fig. 4(a) (right)], a $\pi/2$ pulse at $t = 0$ is followed by a first period of free evolution. Rephasing is induced by a π pulse after t_π . After an additional period of free evolution with variable duration, the sequence is completed by a second $\pi/2$ pulse and detection of the atoms in $F = 2$. The maximum amplitude of the echo signal occurs at $t = 2t_\pi$ ($2t_\pi = 20 \text{ ms}$ in Fig. 4). For the case of transported atoms [Fig. 4(b) (right)], transport over a distance of $55 \mu\text{m}$ takes place during the first 2 ms of the first phase of free evolution with no transport during the second phase. Additional dephasing and decoherence caused by atom transport during the first phase are not compensated during the second phase and should cause a reduction of the signal amplitude at $t = 2t_\pi$. Figure 4 shows that this effect is almost negligible in our system.

For a quantitative investigation, Fig. 5 presents the signal contrast, i.e., the maximum amplitude A_E of the echo signal at $2t_\pi$ normalized to the amplitude of the Ramsey signal $A_R(t = 0)$ for a single central trap as a function of $2t_\pi$ for atoms at rest [5(a)] and atoms transported over $55 \mu\text{m}$ within 2 ms [5(b)]. The loss in signal contrast is clearly nonexponential in both cases. From a detailed

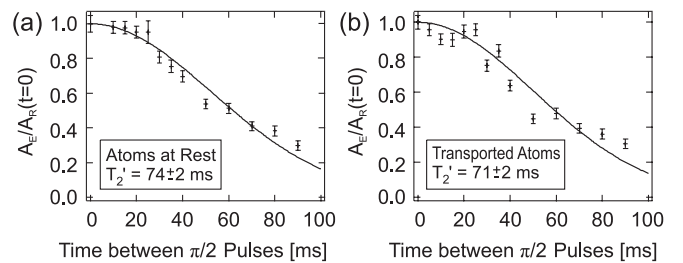


FIG. 5. Determination of the time constant T'_2 for homogeneous dephasing and decoherence for atoms at rest (a) and atoms transported over $55 \mu\text{m}$ in 2 ms (b). Atom transport has an almost negligible effect on dephasing and decoherence.

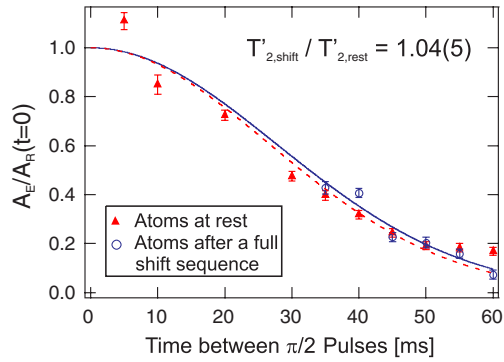


FIG. 6 (color online). Determination of the time constant T'_2 for homogeneous dephasing and decoherence for a full shift register cycle. The signal contrast for atoms at rest (triangles) and atoms after the shift sequence (circles) are shown. The shift sequence has no measurable effect on dephasing and decoherence. Because of imperfect experimental conditions, both absolute time constants T'_2 are smaller than in Fig. 5.

analysis of external influences, we determine homogeneous dephasing due to irreversible variations of the atomic resonance frequency to be the dominant cause for loss of contrast. We identify heating due to photon scattering from the trapping laser with a heating rate too small to be directly observable in Fig. 3(d) to be the most likely cause for this. Following the calculations for homogeneous dephasing given in [25], the signal contrast should be described by the Gaussian function $C(2t_\pi) = C(0) \times \exp[-(2t_\pi)^2/T_2'^2]$ with time constant T_2' for reduction of the initial contrast to its $1/e$ value. The measurements in Fig. 5 can be well fitted to $C(2t_\pi)$ (solid lines), which gives the time constants $T'_{2,\text{rest}} = 74 \pm 2$ ms for atoms at rest, $T'_{2,\text{trans}} = 71 \pm 2$ ms for atoms transported, and a ratio $T'_{2,\text{trans}}/T'_{2,\text{rest}} = 0.96(4)$, which is consistent with 1 within our measurement uncertainty. Thus, atom transport causes almost negligible additional dephasing and decoherence.

We have performed analogous measurements for the sequence of loading and reloading atoms from A1 to A2 and back to A1, and again found no significant decrease in T_2' . Finally, we have investigated dephasing and decoherence for a full shift register cycle. The cycle consists of preparing atoms in A1, transporting them over distance $a/2$, loading them from A1 to A2, and reloading them from A2 to A1. In Fig. 6, the signal contrast for atoms at rest (triangles) and atoms after the shift register cycle (circles) in a single central trap are presented as a function of $2t_\pi$. Fitting both data sets to $C(2t_\pi)$ allows us to extract the ratio $T'_{2,\text{shift}}/T'_{2,\text{rest}} = 1.04(5)$. Thus, also for the full shift register cycle, no additional dephasing or decoherence of internal-state superposition states occurs within the measurement uncertainty. This, by repetition, allows us to build a complete shift register.

In summary, we have presented a novel shift register for atomic quantum systems based on arrays of micro-fabricated lenses. We have demonstrated that transport,

reloading, and a full shift register cycle can be performed with negligible atom loss, heating, or additional dephasing or decoherence. This proves that the fundamental shift sequence can be cascaded and thus scaled to complex and versatile 2D architectures allowing coherent quantum-state storage and transport along complex and reconfigurable paths in 1D and—by simply upgrading our 1D scanner to a 2D version—also in 2D. Together with parallelized site-selective single atom detection [26] and site-selective quantum-state manipulation [14,23,24], novel geometries for quantum information processing, quantum simulation, and multiparticle entanglement become accessible.

We acknowledge financial support by the DFG, by the European Commission (IP SCALA), by NIST (Grant No. 60NANB5D120), and by the DAAD (Contract No. 0804149).

*gerhard.birkl@physik.tu-darmstadt.de

- [1] S. Kuhr *et al.*, *Science* **293**, 278 (2001).
- [2] O. Mandel *et al.*, *Nature (London)* **425**, 937 (2003).
- [3] D. Schrader *et al.*, *Phys. Rev. Lett.* **93**, 150501 (2004).
- [4] I. Bloch, *Nature Phys.* **1**, 23 (2005).
- [5] Y. Miroshnychenko *et al.*, *Nature (London)* **442**, 151 (2006).
- [6] M. Anderlini *et al.*, *Nature (London)* **448**, 452 (2007).
- [7] T. L. Gustavson *et al.*, *Phys. Rev. Lett.* **88**, 020401 (2001).
- [8] R. Dumke *et al.*, *Phys. Rev. Lett.* **89**, 097903 (2002).
- [9] D. D. Yavuz *et al.*, *Phys. Rev. Lett.* **96**, 063001 (2006).
- [10] J. Beugnon *et al.*, *Nature Phys.* **3**, 696 (2007).
- [11] M. P. A. Jones *et al.*, *Phys. Rev. A* **75**, 040301 (2007).
- [12] G. Birkl, R. Dumke, F. B. Buchkremer, and W. Ertmer, *Opt. Commun.* **191**, 67 (2001).
- [13] R. Dumke, T. Mütter, M. Volk, W. Ertmer, and G. Birkl, *Phys. Rev. Lett.* **89**, 220402 (2002); F. B. J. Buchkremer *et al.*, *Laser Phys.* **12**, 736 (2002); A. Lengwenus, J. Kruse, M. Volk, W. Ertmer, and G. Birkl, *Appl. Phys. B* **86**, 377 (2007); G. Birkl and J. Fortágh, *Laser Photon. Rev.* **1**, 12 (2007).
- [14] J. Kruse, C. Gierl, M. Schlosser, and G. Birkl, *Phys. Rev. A* **81**, 060308 (2010).
- [15] D. P. DiVincenzo, *Fortschr. Phys.* **48**, 771 (2000).
- [16] G. K. Brennen, C. M. Caves, P. S. Jessen, and I. H. Deutsch, *Phys. Rev. Lett.* **82**, 1060 (1999).
- [17] D. Jaksch, H.-J. Briegel, J. I. Cirac, C. W. Gardiner, and P. Zoller, *Phys. Rev. Lett.* **82**, 1975 (1999).
- [18] D. Jaksch *et al.*, *Phys. Rev. Lett.* **85**, 2208 (2000).
- [19] T. Calarco *et al.*, *Phys. Rev. A* **61**, 022304 (2000).
- [20] K. Eckert *et al.*, *Phys. Rev. A* **66**, 042317 (2002).
- [21] J. Mompart, K. Eckert, W. Ertmer, G. Birkl, and M. Lewenstein, *Phys. Rev. Lett.* **90**, 147901 (2003).
- [22] D. Hayes, P. S. Julienne, and I. H. Deutsch, *Phys. Rev. Lett.* **98**, 070501 (2007).
- [23] T. Wilk *et al.*, *Phys. Rev. Lett.* **104**, 010502 (2010).
- [24] L. Isenhower *et al.*, *Phys. Rev. Lett.* **104**, 010503 (2010).
- [25] S. Kuhr *et al.*, *Phys. Rev. A* **72**, 023406 (2005).
- [26] M. Schlosser *et al.* (to be published).